



## Faulting and hydration of the Juan de Fuca plate system

Mladen R. Nedimović<sup>a,c,\*</sup>, DelWayne R. Bohnenstiehl<sup>b,c</sup>, Suzanne M. Carbotte<sup>c</sup>,  
J. Pablo Canales<sup>d</sup>, Robert P. Dziak<sup>e</sup>

<sup>a</sup> Department of Earth Sciences, Dalhousie University, Room 3006, Life Sciences Centre, Halifax, NS, Canada B3H 4J1

<sup>b</sup> Department of Marine, Earth and Atmospheric Sciences, North Carolina State University, Campus Box 8208, Raleigh, NC 27695, USA

<sup>c</sup> Lamont–Doherty Earth Observatory of Columbia University, 61 Route 9W, P. O. Box 1000, Palisades, NY 10964-8000, USA

<sup>d</sup> Department of Geology and Geophysics, MS#24, Woods Hole Oceanographic Institution, 360 Woods Hole Road, Woods Hole, MA 02543, USA

<sup>e</sup> Hatfield Marine Science Center, Oregon State University and NOAA, 2030 Marine Science Drive, Newport, OR 97365, USA

### ARTICLE INFO

#### Article history:

Received 20 October 2008

Received in revised form 4 April 2009

Accepted 12 April 2009

Available online 17 May 2009

Editor: R.D. van der Hilst

#### Keywords:

Juan de Fuca plate system  
seismic reflection imaging  
faulting  
hydration  
earthquakes

### ABSTRACT

Multichannel seismic observations provide the first direct images of crustal scale normal faults within the Juan de Fuca plate system and indicate that brittle deformation extends up to ~200 km seaward of the Cascadia trench. Within the sedimentary layering steeply dipping faults are identified by stratigraphic offsets, with maximum throws of  $110 \pm 10$  m found near the trench. Fault throws diminish both upsection and seaward from the trench. Long-term throw rates are estimated to be  $13 \pm 2$  mm/kyr. Faulted offsets within the sedimentary layering are typically linked to larger offset scarps in the basement topography, suggesting reactivation of the normal fault systems formed at the spreading center. Imaged reflections within the gabbroic igneous crust indicate swallowing fault dips at depth. These reflections require local alteration to produce an impedance contrast, indicating that the imaged fault structures provide pathways for fluid transport and hydration. As the depth extent of imaged faulting within this young and sediment insulated oceanic plate is primarily limited to approximately Moho depths, fault-controlled hydration appears to be largely restricted to crustal levels. If dehydration embrittlement is an important mechanism for triggering intermediate-depth earthquakes within the subducting slab, then the limited occurrence rate and magnitude of intraslab seismicity at the Cascadia margin may in part be explained by the limited amount of water imbedded into the uppermost oceanic mantle prior to subduction. The distribution of submarine earthquakes within the Juan de Fuca plate system indicates that propagator wake areas are likely to be more faulted and therefore more hydrated than other parts of this plate system. However, being largely restricted to crustal levels, this localized increase in hydration generally does not appear to have a measurable effect on the intraslab seismicity along most of the subducted propagator wakes at the Cascadia margin.

© 2009 Elsevier B.V. All rights reserved.

### 1. Introduction

Oceanic plates carry physically and chemically bound water into subduction zones (e.g., Peacock, 1990; Meade and Jeanloz, 1991; Moore and Vrolijk, 1992; Ranero et al., 2003). As the subducting oceanic plates descend, and the pressure and temperature rise with the increasing depth, the water stored in the plates is gradually released through a series of dehydration reactions (e.g., Meade and Jeanloz, 1991; Kirby et al., 1996; Peacock, 2001; Hacker et al., 2003a,b). This free water is believed to strongly affect a number of processes important to natural hazard studies. The released water promotes partial melting responsible for arc magmatism (Tatsumi and Eggins, 1995; Kirby et al., 1996), can affect the mechanical characteristics of an interplate interface (Shipley et al., 1994; Nedimović et al., 2003a;

Kodaira et al., 2004), and induces intraslab earthquakes at intermediate depths (~50–300 km) (Raleigh and Paterson, 1965; Meade and Jeanloz, 1991; Kirby et al., 1996).

Significant effort has therefore been directed toward understanding dehydration processes during subduction, with particular emphasis on the influence these processes may have on the depth-distribution of intraslab seismicity (Meade and Jeanloz, 1991; Peacock, 2001; Hacker et al., 2003a,b; Jung et al., 2004). To fully evaluate the importance of slab dehydration, however, it is also necessary to constrain the amount of water bound in the slab when it is subducted at the trench (Ranero et al., 2003). We focus our effort on determining the penetration depth and relative volume extent of oceanic slab hydration offshore Cascadia margin. For this purpose, we process ~1500 km of ridge-flank multi-channel seismic (MCS) data collected in 2002 during the EW0207 cruise and compile a database of seismic reflection profiles from all earlier crustal scale MCS surveys (streamers 2.4 km or longer) across the Juan de Fuca plate system. The spatial distribution of the MCS lines examined is shown in Fig. 1, along with magnetic isochrones (Wilson, 2002) and the locations

\* Corresponding author. Department of Earth Sciences, Life Sciences Centre, Dalhousie University, Edzell Castle Circle, Halifax NS Canada B3H 4J1. Tel.: +1 902 494 4524; fax: +1 902 494 6889.

E-mail address: [mladen@dal.ca](mailto:mladen@dal.ca) (M.R. Nedimović).

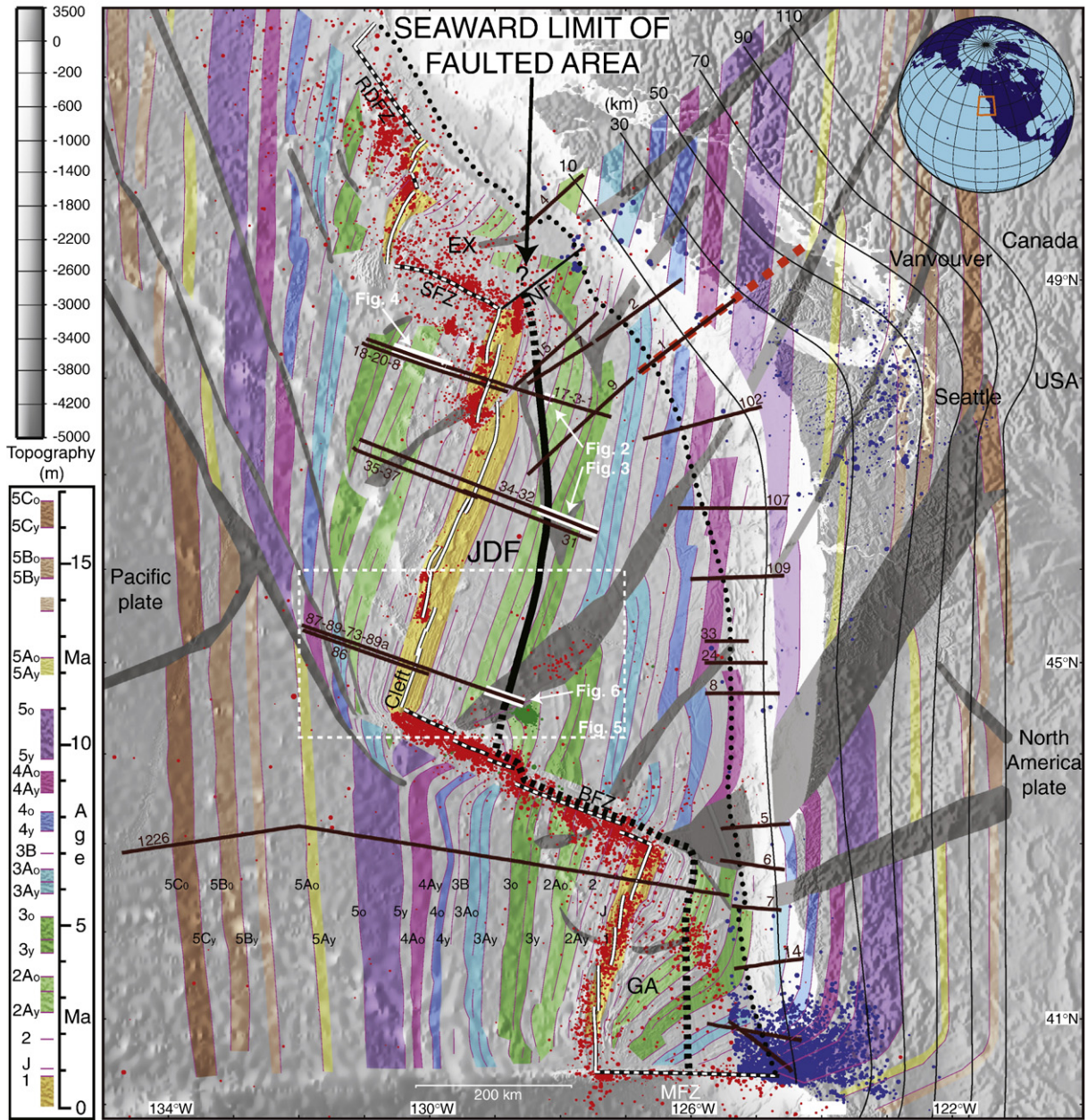


**Fig. 1.** Juan de Fuca plate regional seismicity and crustal age superimposed over grayscale bathymetry. Crustal scale marine MCS profiles from eight regional surveys are shown using thick brown lines. Line numbers are defined as in original surveys. White sections on transects 17-3-1, 34-32 and 87-89-73-89a represent the locations of the images shown in Figs. 2, 3, 4 and 6 respectively. Dashed white rectangle outlines the area shown in Fig. 5. Thick dashed orange line shows the location of the thermal profile of Wang et al. (1995) crossing the northern Cascadia margin. Thick black line on the subducting plates outlines the seaward limit of the region of extension or transtension where normal faulting is observed (solid) or inferred (dashed). Dotted black line shows the location of the trench. Long N-trending black isodepth lines (McCrorry et al., 2004) show the position of the Juan de Fuca oceanic slab beneath North America. Red dots are earthquakes recorded from 1991 to 2004 by the Sound Surveillance System (SOSUS) (Fox et al., 1994; <http://www.pmel.noaa.gov/vents/acoustics/autchart/GetPosit.html>). Blue dots are intraslab earthquakes with magnitudes >2 recorded from 1975 to 2002 and extracted from the Advanced National Seismic System catalog (McCrorry et al., 2004). Green dots near the eastern end of transect 87-89-73-89a represent the SOSUS-detected earthquake swarm from April 2008. White lines with black edges are the interpreted traces of the ridge axis; dashed over fracture zones. Thin pink lines are magnetic isochrons that outline color shaded magnetic anomalies 1 through 5C, and grey shading outlines propagator wakes (Wilson, 1988; 2002). JDF–Juan de Fuca plate; EX–Explorer plate; GA–Gorda deformation zone; RDFZ–Revere–Dellwood fracture zone; SFZ–Sovanco fracture zone; NF–Nootka fault; BFZ–Blanco fracture zone; MFZ–Mendocino fracture zone. Inset in the upper right corner shows the location of the study area with respect to North America.

of Cascadia margin earthquakes believed to be spatially restricted to the Juan de Fuca plate and subducting slab (Fox et al., 1994; McCrorry et al., 2004).

**2. Study area**

The study area shown in Fig. 1, located offshore western North America, encompasses the Juan de Fuca ridge and plate system (Explorer, Juan de Fuca and Gorda ridges and plates), Cascadia de-

formation front, Nootka fault, and Sovanco and Blanco fracture zones. The Juan de Fuca ridge system, a NNE-oriented intermediate-rate spreading center, is located at the boundary between the Pacific plate and the Juan de Fuca plate system. The full spreading rate along the Juan de Fuca ridge is 56 mm/yr, and 56 mm/yr and less along the Explorer and Gorda ridges (e.g., Wilson, 1993). The Cascadia deformation front marks the surface trace of the interface between the Juan de Fuca and North America plates. The Nootka fault is the boundary between the Explorer and the Juan de Fuca plates, and

Blanco and Sovanco fracture zones separate parts of the Juan de Fuca plate system from the Pacific plate.

Both the western and eastern flanks of the Juan de Fuca ridge system are crossed by propagator wakes but otherwise show prominent differences indicating that they are evolving in a markedly different way due to distinct sedimentary and volcanic histories. Seamounts, which are found primarily on the Pacific plate, occur as isolated edifices and in chains, several of which lie close to and intersect the Juan de Fuca ridge axis (Davis and Karsten, 1986). Sediments covering the eastern Juan de Fuca ridge flank are up to a few kilometers thick at the northern Cascadia subduction deformation front and thin toward the ridge axis and southward away from the dominant source of terrigenous sediment (Nedimović et al., 2008). The western Juan de Fuca ridge flank is more sparsely sedimented, although sediment cover generally increases to the north where significant sediment accumulation is confined to mini-basins between large basement outcrops. The enhanced accumulation of sediment on the eastern flank is in large part caused by the morphology of the Juan de Fuca ridge, with its cooling and subsiding flanks forming basin-like depositional environments and its elevated axial region acting as a barrier that inhibits the transport of terrigenous sediment to the western flank.

### 3. Reflection imaging

Summary information and corresponding references that describe the MCS data used in this study are provided in Table 1. The prestack processing strategy adopted for the EW0207 MCS data consisted of: standard straight-line CMP bin geometry; F-K and bandpass (2–7–100–125 Hz) filtering to remove the low frequency cable noise; amplitude correction for geometrical spreading; surface consistent minimum phase predictive deconvolution to balance the spectrum and remove short period multiples; surface consistent amplitude correction to correct for anomalous shot and receiver-group amplitudes not related to wave propagation; trace editing; velocity analysis using the velocity spectrum method; normal moveout and dip moveout corrections to align signal for stacking; and CMP mute to remove overly stretched data. Crossdip moveout correction (Nedimović et al., 2003b) was not required because streamer feathering was small ( $<10^\circ$ ) and structural crossdip negligible. The prepared prestack data, with and without the automatic gain control, were then stacked (averaged). The poststack processing included seafloor mute, primary multiple mute to reduce migration noise, bandpass filtering (2–7–100–125 Hz), and time migration to collapse diffractions and position the recorded reflection events to their true subsurface locations. To improve imaging

within the oceanic plate below the upper crust, the late travel time data were additionally bandpass filtered at 2–7–20–40 Hz and mildly coherency filtered.

Analyzed seismic images from field programs other than the 2002 Juan de Fuca cruise were formed earlier by other researchers in a similar way as described for the EW0207 cruise. Specific details about the processing stream are provided in Calvert and Clowes (1991) for the 1985 Frontier Geoscience project, in Calvert (1996) for the 1989 ODP Leg 146 site survey offshore Vancouver Island, in MacKay et al. (1992) for the 1989 ODP Leg 146 site survey offshore Oregon, in Flueh et al. (1998) for the 1996 Orwell project, and in Gulick et al. (1998) for the 1994 Mendocino Triple Junction experiment. The 1994 Gorda Rise and Cape Blanco data were processed only to near-offset brute stacks (Brocher et al., 1995; <http://www.ig.utexas.edu/sdc/cruise.php?cruiseIn=ew9413>). This processing included: trace edit, amplitude recovery, bandpass filter, CMP sort, normal moveout, stretch mute and stack. From the various survey campaigns described here only some of the Orwell project profile data, although collected using the shortest streamer (2.4 km) with the smallest number of channels (48), were prestack depth processed (Flueh et al., 1998).

### 4. Characterization of faulting

Analysis of the compiled database of seismic reflection images (Fig. 1) resulted in an outline of the Juan de Fuca plate region of extension or transtension, where normal faulting is observed (Fig. 1). The faulting appears nearest to the ridge axis at the northern end of the Juan de Fuca plate but the width of the faulted zone seems to increase southward along the trench, reaching a maximum of over 200 km near the Blanco fracture zone. Both Explorer and Gorda plates experience deformation throughout, as indicated by the seismicity (Fig. 1). However, seismic reflection constraints on the extent of normal faulting in these two areas are rather limited due to the lack of profile coverage or insufficient image resolution.

In Fig. 2 we show for the first time a reflection image of faults within the Juan de Fuca plate system that extend all the way through the sediments and crust to about the Moho discontinuity. The imaged faults are spatially tied to ridge-parallel fault structures that represent pre-existing zones of weakness. Fault offsets gradually diminish upsection with sediment age, suggesting growth faulting caused by repeated slip on basement structures (Figs. 2 and 3). Our reflection image resolution permits identification of fault-plane sections within the sediments with throws  $>2$ –3 m. This resolution estimate is governed by the data sample rate (2 ms), sediment interval velocities (1550–3300 m/s), and frequency content of the signal (from  $\sim 2$  Hz to over 100 Hz). Therefore, based only on the reflection images, we

**Table 1**

Summary information characterizing seismic reflection data from all crustal scale MCS surveys with streamers 2.4 km or longer across the Juan de Fuca plate system.

Project name & year	Profiles used in this study	Streamer length & type	Channels: number & spacing	Airgun array & volume	Shot spacing	Record length & sample rate	CMP spacing & fold	References
Juan de Fuca, EW0207 (2002)	17-3-1, 18-20-8, 34-32, 35-37, 31, 87-89-73-89a, 86	6 km, digital	480, 12.5 m	10-element, 49.2 L	37.5 m	10.24 s, 2 ms	6.25 m, 80	Nedimović et al. (2005)
Canadian Frontier Geoscience Project (1985)	1, 2, 4, 7, 9	3 km, analogue	120, 25 m	108.3 L	50 m	16 s, 4 ms	12.5 m, 30	Calvert and Clowes (1991)
ODP Leg 146 site survey, Vancouver Island (1989)	15	3.6 km, analogue	144, 25 m	128.2 L	50 m	16 s, 4 ms	12.5 m, 36	Calvert (1996)
ODP Leg 146 site survey, offshore Oregon (1989)	8, 24, 33	3.6 km, analogue	144, 25 m	128.2 L	25 m	8 s, 4 ms	12.5 m, 72	MacKay et al. (1992)
Orwell Project, SOONE SO108 (1996)	102, 107, 109	2.4 km, analogue	48, 50 m	87.4 L	50 m	16 s, 4 ms	25 m, 24	Flueh et al. (1998)
Gorda Rise, EW9413 (1994)	1226	4 km, digital	160, 25 m	20-element, 137.5 L	50 m	12 s, 2 ms	12.5 m, 40	*UTIG web pages
Cape Blanco, EW9414 (1994)	5, 6, 7	4 km, digital	160, 25 m	10-element, 49.2 L	50 m	14 s, 2 ms	12.5 m, 40	Brocher et al. (1995)
Mendocino Triple Junction, EW9407 (1994)	3, 6, 14	4 km, digital	160, 25 m	10-element, 49.2 L	50 m	14 s, 2 ms	12.5 m, 40	Gulick et al. (1998)

\*<http://www.ig.utexas.edu/sdc/cruise.php?cruiseIn=ew9413>.

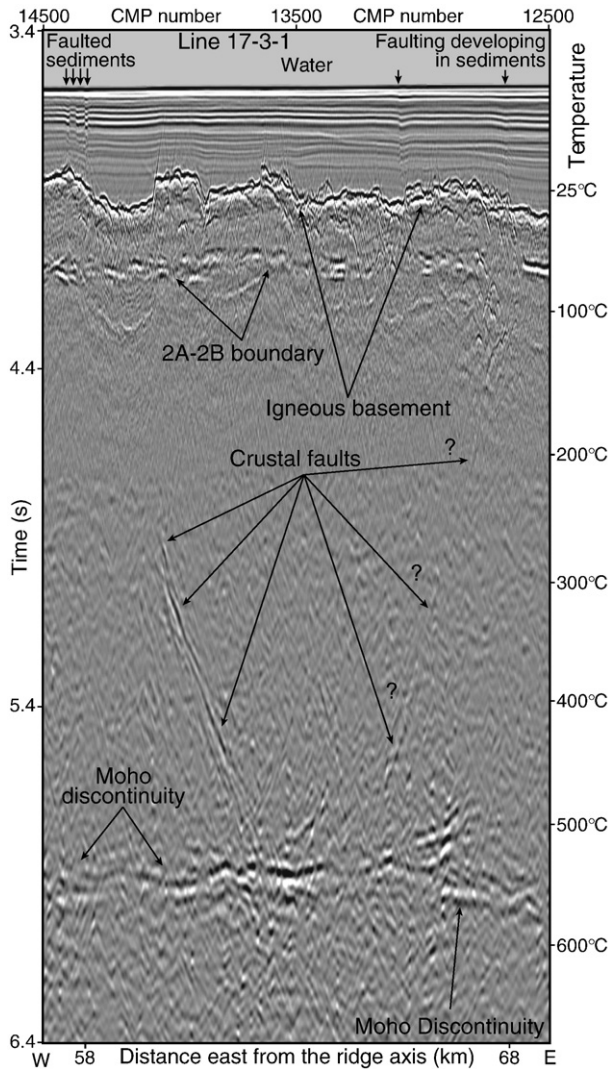


**Fig. 2.** Seismic reflection image of normal faults rooted near the Moho discontinuity and extending through the crust and the overlying sediments is extracted from transect 17-3-1 (see Fig. 1 for location). Such direct imaging of normal faulting in young oceanic plates from seafloor to Moho is not common because normal fault planes dip steeply and generally appear transparent for the seismic reflection method. Temperatures on the right side are derived from a half-space cooling model for 2.75 Ma-old oceanic crust assuming thermal diffusivity  $\kappa = 0.804 \times 10^{-6} \text{ m}^2/\text{s}$  and initial temperature  $T_m = 1300 \text{ }^\circ\text{C}$ . To simulate the impact of sedimentation, the temperature at the sediment–basement interface is constrained as  $T_s = 25 \text{ }^\circ\text{C}$ , which assumes an average sediment thickness of 250 m as plate ages and a  $0.1 \text{ }^\circ\text{C}/\text{m}$  thermal gradient in the sediments. Advanced 1D and 2D finite-element models of Juan de Fuca plate temperatures for areas closer to the trench and within the subduction zone can be found in Wang et al. (1995) and Hyndman and Wang (1993, 1995).

cannot conclude whether the lack of visible faulting within the topmost sediments (Fig. 3) is due to the limited image resolution, or due to the absence of recent dip slip displacement on these structures.

To resolve this, we first estimate the maximum long-term fault-throw rates for the study area and then compare them with the recent sedimentation rates. Maximum fault throws of  $110 \pm 10 \text{ m}$  are observed offshore Oregon, just west from the trench along the ODP Leg 146 line 8. The shortest distance seaward from this fault toward the onset of faulting is  $200 \pm 20 \text{ km}$ , and the half spreading rate is  $28 \text{ mm}/\text{yr}$  (e.g., Wilson, 1993). This information yields a maximum long-term throw rate of  $15 \pm 2 \text{ mm}/\text{kyr}$ . We also estimate the same parameters along the 2002 Juan de Fuca survey transect 17-3-1 offshore Vancouver Island/Olympic Peninsula that spatially coincides with the Endeavour ODP/IODP drilling transect, and for which there is a wealth of information about the sedimentation rates. Maximum

identified throw along this profile is  $20 \pm 2 \text{ m}$ ; trench-normal distance between the maximum throw fault and the seaward onset of faulting is  $50 \pm 5 \text{ km}$ ; and the half spreading rate is also  $28 \text{ mm}/\text{yr}$ . These data yield a maximum long-term throw rate of  $11 \pm 2 \text{ mm}/\text{kyr}$ . The two calculated long-term throw rates agree within the error limits and combined give an average long-term throw rate for the imaged normal faults along the Juan de Fuca plate of  $13 \pm 2 \text{ mm}/\text{kyr}$ . This long-term throw-rate estimate is more than 25 times smaller than the rapid average sedimentation rate of  $\sim 336 \text{ mm}/\text{kyr}$  obtained for the time-stratigraphic period A characterizing the past 90 kyr along the Endeavour ODP/IODP drilling transect (Underwood et al., 2005). The topmost sediments accumulated during the time-stratigraphic period A have an average thickness of some 30 m while the estimated cumulative fault throw during this period is  $1.17 \pm 0.18 \text{ m}$ , less than the resolution threshold for our images. This suggests that plate-deforming processes have remained active during most recent geologic time with the resulting normal faulting displacing the whole sediment column.

Fault throws show no reversals in slip direction and gradually increase both downsection, from younger to older sediments, and toward the trench with increasing crustal age. Observations of compaction-induced sediment folding without faulting at places where there are large offsets in the basement structure (e.g., Fig. 3 at  $\sim 125 \text{ km}$ ; Fig. 4 at  $\sim 85 \text{ km}$ ; Figs. 5 and 6 at  $\sim 120 \text{ km}$ ) suggests that the sediment rupture is not caused by compaction, but rather by movement of basement fault systems. Particularly supportive of this interpretation is the Fig. 4 reflection image of the section of transect 17-3-1 showing significant sediment accumulation on the western Endeavour ridge flank. Folding of sedimentary strata due to differential compaction over the rough igneous basement is present throughout the mini-basins but no faulting can be observed despite the large, up to a few hundred meters high steps in the basement structure. These mini-basins extend to more than 110 km west from the Endeavour ridge axis, significantly farther than the distance east from the Juan de Fuca ridge axis (55–110 km) at which the seaward limit of faulting is observed on all transects (Figs. 1–3, 6). Moreover, sediment thickness in the mini-basins over the western Endeavour ridge flank (Fig. 4) is twice that on the eastern Endeavour flank at the seaward limit of faulting (Fig. 2), further indicating that the faulting is caused by movement of basement fault systems and not differential compaction. However, faulting in the sediments where there are only small offsets in the basement implies that faulting does not in all cases occur at the pre-existing planes of weakness formed at the Juan de Fuca ridge system.

The growth-fault interpretation is in general in agreement with the existing lithospheric stress models for the Juan de Fuca plate system (Wang et al., 1997). Nevertheless, the intraplate stress regime for the Juan de Fuca plate system is known to be complex, with variable distribution of compressive and tensile stresses, and it is possible that many of the described faults may have also experienced transcurrent motion. Based on reflection images of the sediments (MacKay et al., 1992; Gulick et al., 1998), and from earthquake studies and high-resolution images of the seafloor (Chaytor et al., 2004), strike-slip and normal faulting have both been suggested for the Gorda and southern part of the Juan de Fuca plate. Our images are 2D and sparsely distributed thus providing no constraints on transcurrent motion along the imaged faults.

Crustal faulting within young oceanic plates is in most cases inferred from offsets observed at the igneous basement or within the overlying sediments, as shown in Fig. 3. Fig. 2 is exceptional because it shows reflections from the fault planes that can be identified within the lower half of the image, or the lower two-thirds of the igneous oceanic crust assuming average crustal velocities. The deep faulting projects to offsets in the igneous basement and sediments indicating that the faults transect the whole crust. This suggests that the imaged faults are listric—too steep to be imaged in the shallow-most crust, and sloping gently enough to be imaged at greater depth.

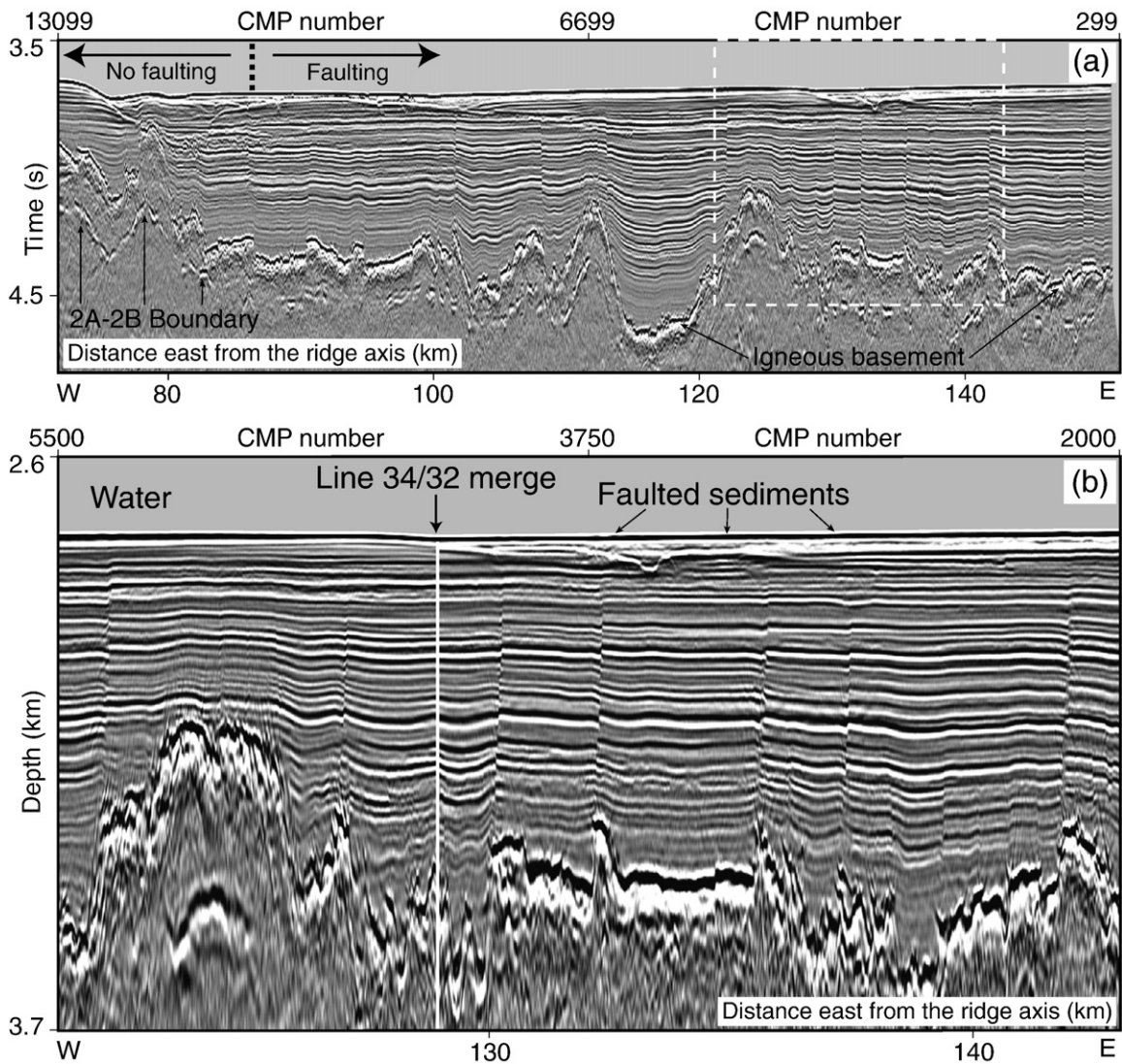


**Fig. 3.** Seismic reflection images showing normal faulting within the sediments at the eastern end of transect 34-32. Also visible in the sections are the igneous basement reflection and the layer 2A/2B event that is believed to mark the location of the upper crustal interface between the extrusives and sheeted dikes. (a) An 80 km-long section of transect 34-32 (see Fig. 1 for location) depicting the gradual westward transition from faulted to not faulted sediments. The white dashed box in (a) outlines the location of the detailed image of faulting shown in depth in (b). Conversion from twtt to depth was done along vertical rays using interval velocities. The discontinuity marked by a vertical white line in (b) at the distance of ~129 km is at the location where lines 34 and 32 were merged.

Crustal reflections can potentially also be caused by varying mineralogical content (e.g., of plagioclase) inherited from axial igneous processes; however, the geometry of the boundary between crustal zones of different mineralogical content is unlikely to both a) be identical to that caused by normal faulting and b) spatially correlate with the position of basement scarps and faulting in the sediments. Furthermore, the sharp changes in crustal mineralogical content needed to produce imageable reflections are not common in nature, at least not in our study area where images of the oceanic crust are void of any reflectivity excluding the top of the igneous crust and Moho events, and the small number of fault-related steeply dipping events discussed in this work.

The imaged fault reflections are not migration or other artefacts because their geometrical shape does not resemble that of migration 'smiles', they extend over a very long distance through the sections, and they project onto the displaced sediments. Moreover, the seismic sections formed using data collected during the 2002 Juan de Fuca cruise are of high signal-to-noise ratio (Nedimović et al., 2005) and are generally void of seismic noise that could be misinterpreted as fault reflections. Primary multiples are very strong and limit the depth to which the obtained images can be interpreted. In Fig. 2, primary

multiples arrive at about 7 s two-way traveltime. We show this section to 6.4 s two-way traveltime because the deeper portion to 7 s is affected by primary multiples migration noise.

The observed fault reflections returning from within the mostly gabbroic oceanic crust and mostly peridotitic uppermost mantle are possible only if the rocks along the fault surfaces are altered to produce an acoustic impedance contrast. As these alteration products require the availability of seawater, this indicates that the extensional faults along the Juan de Fuca plate system are conduits for fluids and that their observed depth extent in the reflection images should constrain the local depth limit of plate hydration. The depth of imageable fault penetration correlates well with the 500–600 °C isotherm and is approximately coincident with the location of the Moho reflection (Fig. 2). At greater depths and therefore greater temperatures, serpentinization, the most important hydration mechanism for peridotites, becomes a marginal process (Ulmer and Trommsdorff, 1995). The lowest Juan de Fuca plate temperatures are expected along the Oregon Margin (8–10 Ma crust); however, due to the increasing accumulation of an insulating and heat producing sediment layer, thermal models predict that Moho temperatures will remain high (450–500 °C) as the plate enters the trench (Hyndman

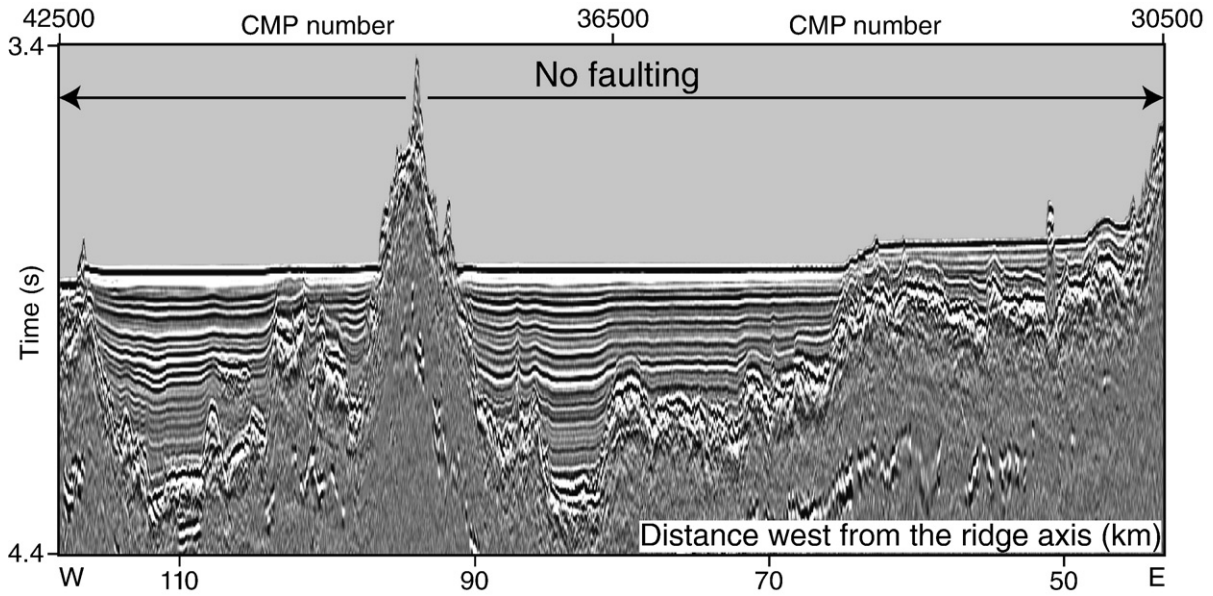


**Fig. 4.** Reflection image of the section of transect 17-3-1 showing significant sediment accumulation confined to mini-basins found on the western Endeavour ridge flank. Folding of sedimentary strata due to differential compaction over the rough igneous basement is present throughout the mini-basins, but no faulting can be observed although the steps in the basement reach up to a few hundred meters.

and Wang, 1993, 1995; Wang et al., 1995). Therefore, it appears that prior to subduction only the uppermost Juan de Fuca mantle can become hydrated by peridotite “corrosion” to serpentinite, despite the pervasive extensional faulting imaged seaward of the trench (Figs. 2 and 3).

After subduction, increased pressure may cause the antigorite stability region to initially increase as the slab starts to descend (e.g., Wada et al., 2008). Provided fault systems maintain permeability, free water within the plate could facilitate additional and deeper serpentinization of the mantle rocks during this time. This process is expected to be common to all slabs; however, its extent cannot be assessed readily from reflection imaging. Dehydration occurs during later stages of subduction in response to slab warming.

**5. Comparisons and implications**

The only other convergent margin with both seismic reflection evidence for the depth extent of faulting and thermal modelling results is the Middle America subduction zone (Ranero et al., 2003; Harris and Wang, 2002). Normal faulting offshore Middle America margin covers a narrower swath of seafloor (~60 km) but is more pronounced than offshore Cascadia margin where the faulted area is wider (100–250 km). The width of the faulted area offshore Middle America appears consistent with the 40–75 km wide area estimated from lower resolution single-channel seismic and sidescan images from the outer-rise region of other subduction zones (e.g., Masson, 1991). The anomalously wide zone documented on the Juan de Fuca plate may indicate that the stress field within this small plate is not controlled solely by plate bending, but includes contributions from thermal contraction and basal shear, as well as ridge and transform push (Wang et al., 1997). Fault fabric inherited from crustal accretion at the ridge also has relatively little time to heal and may therefore be reactivated even under small differential stresses found at a great distance from the trench. Alternatively, the faulting offshore Middle America margin (and elsewhere) may start at a greater distance from the trench than observed, but the combination of slower sedimentation rates and few available high quality MCS reflection images makes it impossible to resolve faults with throws smaller than ~10–20 m with the existing data.

Faults are imaged to depths of ~6–7 km within the Juan de Fuca plate system. Although there are currently no seismic reflection constraints on the depth extent of alteration along fault planes within the oldest portions of the plate near the Cascadia margin, thermal modelling (Hyndman and Wang, 1993, 1995; Wang et al., 1995) indicates that serpentinization should extend no more than a few kilometers into slab mantle. At the Middle America trench, however, faults are imaged to depths of ~20–22 km, some 15 km into the upper mantle. Like at the Cascadia margin, the depth of imageable fault penetration at the Middle America trench correlates well with the 500–600 °C isotherm from thermal models. The Middle America outer-rise fault density gradually increases toward the trench reaching ~8 faults per 5 km. Fault density at the Cascadia margin, although variable, is comparatively low across the faulted area with ~1–2 faults per 5 km trench-normal distance. While fault throws at the Middle America trench can reach ~500 m, those adjacent to the Cascadia trench exhibit maximum offsets of only ~110 m. These differences in fault density, fault throws, and imageable depth of fault penetration suggest that the amount of water bound in the

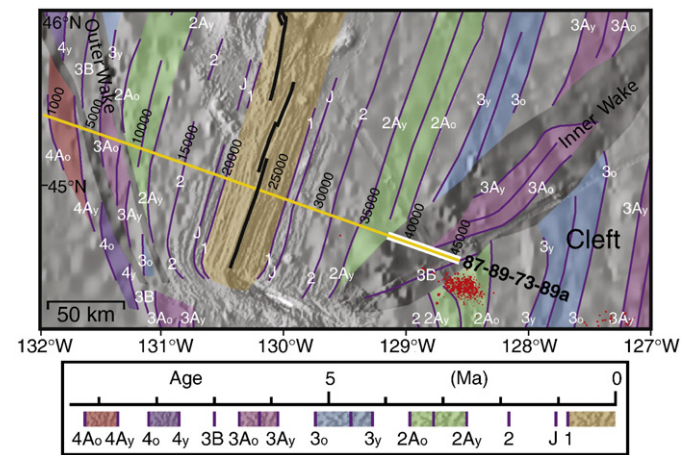


**Fig. 5.** Earthquake swarm of 2008 (red dots) superimposed over crustal age and grayscale bathymetry of the Cleft ridge segment (see Fig. 1 for location). Orange solid line is MCS transect 87-89-73-89a from the EW0207 cruise. Reflection image of the transect section underlined with a thick solid white line is shown in Fig. 6.

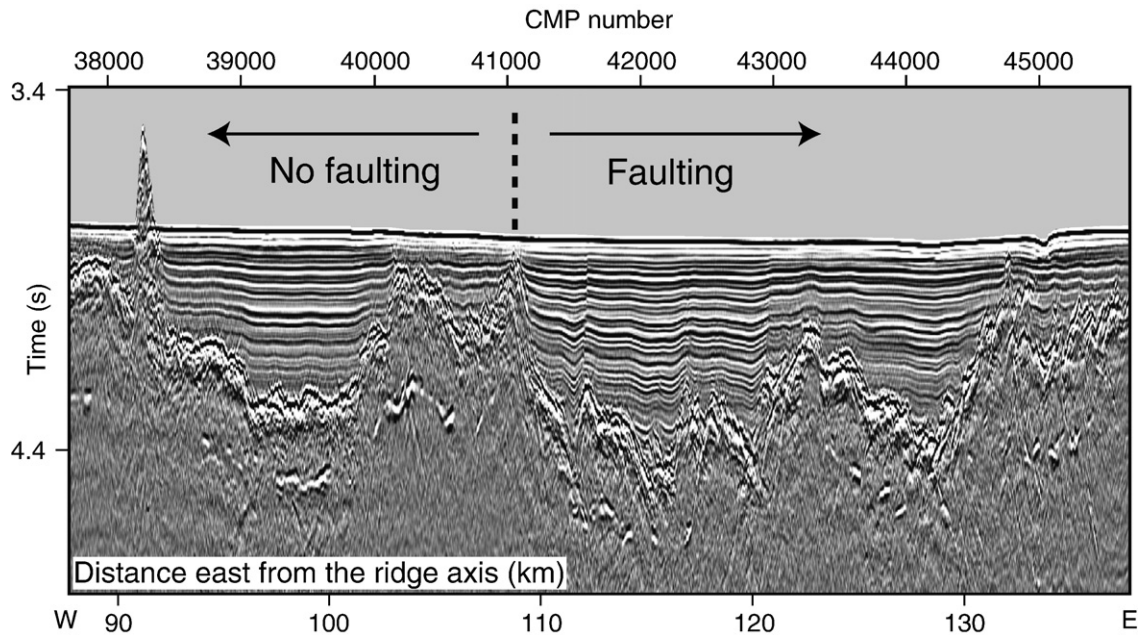


**Fig. 6.** Seismic reflection image showing the approximate location of the landward onset of faulting at the eastern end of transect 87-89-73-89a (see Figs. 1 and 5 for location). The earthquake swarm shown in Fig. 5 partially overlaps the faulted section and extends further east.

subducting slab at the Middle America trench is significantly greater than that at the Cascadia margin. Specifically, the contribution from serpentinized upper mantle rocks, which is equivalent to a 0.17–1.7 km-high column of water per unit length at the Middle America trench (Ranero et al., 2003), appears to be largely absent along Cascadia. This missing volume rivals the amount of water stored in the igneous oceanic crust (Moore and Vrolijk, 1992).

Much attention has been given to the role of dehydration embrittlement in triggering intermediate-depth earthquakes within the subducting slab and the localization of these seismic events on pre-existing fault sets (Raleigh and Patterson, 1965; Yamasaki and Seno, 2003; Hacker et al., 2003b). As shown in Fig. 1, intraslab seismicity at the Cascadia margin is sparse and shallow (<~80–90 km), and focused in only a few areas—the southern margin of the slab near the Mendocino triple junction, the eastern Olympic peninsula region, and to a lesser extent the area beneath mid-western Vancouver Island (Fig. 1). The largest recorded intraslab events occur in a small area offshore northern California, have shallow hypocenters (<20 km depth), strike-slip mechanisms, and moment magnitudes of up to ~7.3 (Wong, 2004). The largest intermediate-depth intraslab earthquakes occur onshore across the northern Cascadia subduction zone. Their observed maximum moment magnitudes are ~6.8 (April 23, 1949 Olympia and February 28, 2001 Nisqually earthquakes) (Malone, 2001; Rogers and Crosson, 2002). In the case of the 2001 Nisqually earthquake (slab age ~10 Ma at the time of subduction), waveform analysis suggests that the rupture occurred on a steeply dipping plane that spanned the lower oceanic crust and extended no more than 10 km into the subducted mantle (Kao et al., 2008). This is consistent with the idea that as antigorite dehydration begins and fluids migrate upward, the maximum depth extent of the embrittled mantle region is limited by the original depth of hydration. By comparison, the maximum moment magnitude for analogous, intermediate-depth events recorded at the Middle America margin, which is characterized by abundant and deeper reaching (300 km) intermediate depth seismicity, is nearly a full magnitude unit larger (Seno and Yoshida, 2004). For the largest recorded event, the January 13, 2001 El Salvador earthquake ( $M_w$  7.7), significant moment release is observed along a steeply (60°) dipping plane with a down-dip dimension of roughly 25 km, extending well into the subducted upper mantle (Vallée et al., 2003).

The maximum depth of intraslab seismicity is well known to correlate with slab thermal parameter, the product of slab age and subduction rate (Kirby et al., 1996). This is commonly interpreted to reflect the temperature-dependent locus of dehydration within metamorphosed oceanic crust and serpentinized slab mantle (Raleigh and Paterson, 1965; Peacock, 2001; Hacker et al., 2003a,b). However, MCS observations also show that the dense and deep-cutting faulting of the older (14–24 Ma), colder and thicker (50–55 km) downgoing Cocos plate at the Middle America trench provides a mechanism to embed into the oceanic plate a volume of water much greater than that for the young (4–10 Ma), warm and thin (30–35 km) Juan de Fuca plate. This enhanced availability of water may create an environment more prone to brittle failure once the dehydration processes start. Moreover, water bound within the Cascadia slab is mostly contained within the hydrous crustal mineral phases, rather than serpentinized mantle peridotite, which remains stable at higher temperatures (greater depths) within the slab (Yamasaki and Seno, 2003; Hacker et al., 2003b). Deep fault penetration into the Cocos plate at the Middle America trench also creates pre-existing zones of weakness with larger surface area relative to those at the Cascadia margin, leading to higher potential for larger magnitude intraslab earthquakes.

In addition to the low frequency of intraslab earthquakes beneath Cascadia, relative to Middle America, we note that the sparse seismicity of the slab is clustered tightly within the northern and southern portions of the plate (Fig. 1). The uniform thickness and structure of Juan de Fuca crust formed along the spreading center (Nedimović et al., 2005) suggests that these clusters may be caused by anomalous hydration of the lithospheric plate as it ages and/or by larger intraslab differential stresses. In this regard, the northward migration of the Mendocino Triple Junction and the accompanying retreat of the slab (Furlong and Schwartz, 2004) may create anomalous stress conditions along the southern margin of the plate. The Mendocino transform zone also may be cooled more rapidly than the rest of the plate due to a thermal boundary effect (e.g., Loudon and Forsyth, 1976) caused by juxtaposition of the old and cold Pacific plate and the young and warm Gorda plate, allowing deeper and more extensive hydration along this long-lived fault zone. Further facilitating hydration of the oceanic plate in this area are two sets of crossing faults observed in reflection profiles (Gulick et al., 2001). The internally deforming and fragmenting southern Gorda plate is rotating clockwise toward the

Mendocino triple junction. This causes the incoming ridge fabric to be oriented at a high angle to the trench (Fig. 1). When the strike of the incoming oceanic spreading fabric forms an oblique angle ( $>20\text{--}30^\circ$ ) with the trench, a new set of trench-parallel faults is formed (Masson, 1991) providing fluid pathways into the oceanic plate in addition to those formed at the spreading center and reactivated near the trench.

In the north, intraslab stresses are influenced by interactions with the Nootka transform fault, which plunges beneath mid-western Vancouver Island (Fig. 1), and by the sharp along-strike bending of the slab beneath Olympic Peninsula. The trench bends westward in this area and, like at the southern Gorda plate, becomes oblique to the ridge tectonic fabric. Therefore, it is possible that two-directional faulting and associated enhanced plate hydration also take place in this northern locality but without new MCS data this cannot be validated.

## 6. Effect of propagator wakes

We also investigate the spatial relationship between the location of propagator wakes and the distribution of seismicity within both the Juan de Fuca plate system and the subducted oceanic slab at the Cascadia margin. While the smaller Explorer and Gorda plates show evidence of seismicity, and presumably active faulting, throughout much of their interior [e.g., Fox and Dziak, 1999; Dziak, 2006], earthquakes located within the Juan de Fuca plate are concentrated along a broad NE-trending propagator wake crossing the eastern Cleft ridge flank (Fig. 1). This region includes a swarm of  $>600$  SOSUS-detected events recorded in April 2008, positioned near  $44^\circ\text{N}/128^\circ\text{W}$  (Figs. 1 and 5). The affected area is located near the eastern end of our seismic transect 87-89-73-89a. Analysis of the seismic reflection image formed along this 300 km-long transect shows that the only observable faulting in this profile spans the area crossing this propagator wake (Fig. 6). These observations suggest that propagator wakes, as potential zones of plate weakness inherited from crustal accretion, may respond to increasing external stresses by brittle failure earlier and to a greater extent than other parts of oceanic plates. Therefore, the identified faulting and associated earthquake activity indicate that propagator wakes also may be areas of more pervasive plate hydration. As such, these structures should after subduction correlate with zones of elevated intraslab seismicity, assuming that dehydration embrittlement is an important mechanism for triggering intermediate-depth earthquakes within the subducting slab.

Analysis of Fig. 1, however, shows that at the Cascadia margin there does not appear to be a regional correlation between the inferred location of propagator wakes within the subducted oceanic slab and the location of anomalous intraslab seismicity. Despite the increased faulting of the Juan de Fuca plate along the propagator wakes, high temperatures within this young and sedimented oceanic plate may generally limit hydration of even the uppermost mantle such that additional hydration of the propagator areas is limited in volume.

Locally, on the other hand, the propagator wake inferred beneath Olympic Peninsula does appear to spatially correlate with the largest concentration of intraslab seismicity at the northern Cascadia margin. Magnetic isochrons (Fig. 1) suggest that the oceanic plate in this area may be older than in any other section of the subducted Juan de Fuca plate system found at about the same distance from the trench. Taking into account the N–S variability in the recent Cascadia margin convergence rates (e.g., 29 mm/yr at the Oregon–Washington border, 40 mm/yr at the Juan de Fuca Strait; Wells et al., 2002), this section of the subducted plate exhibiting intraslab seismicity was likely the oldest and therefore the coldest when it was at the trench. This, combined with additional fluid pathways within the propagator wake area, likely facilitated deeper and more extensive mantle hydration

than elsewhere in the subduction zone and may contribute to the locally elevated intraslab seismicity rate.

## 7. Summary

MCS data from EW0207 cruise provide the first direct imagery showing crustal scale faulting within the Juan de Fuca plate. Steeply dipping faults within the sedimentary layering are identified by stratigraphic offsets, with dip slip motion decreasing upsection. Imaged faults are generally spatially tied to larger offset scarps in the basement topography, suggesting reactivation of the normal fault systems formed at the spreading center. The analysis of EW0207 data, combined with reflection images within the area from earlier data, was used to map the extent of the Juan de Fuca plate region affected by normal faulting. The mapped region of recent faulting appears to extend to distances of  $>200$  km from the trench.

Imaged reflections within the gabbroic igneous crust indicate swallowing fault dips at depth. These reflections require local alteration to produce an impedance contrast, suggesting that these structures provide pathways for fluid transport and hydration. As the depth extent of imaged faulting within this young and sediment insulated oceanic plate is primarily limited to approximately Moho depths (temperatures reach  $500\text{--}600^\circ\text{C}$ ), fault-controlled hydration is for the most part restricted to crustal levels. Hydration of a thin layer of the uppermost mantle is most likely for sections along the trench where the coldest and anomalously faulted parts of the Juan de Fuca plate system are subducted. If dehydration embrittlement is an important mechanism for triggering intermediate-depth earthquakes within the subducting slab, then the limited occurrence rate and magnitude of intraslab seismicity at the Cascadia margin may in part be explained by the limited amount of water imbedded into the uppermost oceanic mantle prior to subduction.

The distribution of earthquakes within the Juan de Fuca plate system, including the 2008 earthquake swarm, indicates that propagator wake area is likely to be more heavily faulted and therefore more hydrated than other parts of oceanic plates. However, being mostly restricted to the crust, this additional hydration does not appear to have an effect on the distribution and magnitude of the intraslab seismicity at the Cascadia margin except, perhaps, for the anomalous area below the Olympic Peninsula.

## Acknowledgements

This work was made possible through the generosity of American (T. M. Brocher, J. B. Diebold, A. M. Trehu), Canadian (K. Vasudevan) and German (E. Flueh, D. Klaeschen) researchers who provided seismic reflection data. D. S. Wilson kindly supplied magnetic isochron information and critically reviewed the manuscript. We are grateful to M. Protti, L. R. Sykes and G. A. Abers for comments on earlier drafts of this work, which was supported by the Doherty Foundation and the National Science Foundation under grants OCE002488 and OCE0648303 to SMC and MRN.

## References

- Brocher, T.M., Davis, M.J., Clarke, S.H., Geist, E.L., 1995. Onshore-offshore wideangle seismic recordings in October 1994 near Cape Blanco, Oregon. U.S. Geological Survey Open-File Report 95-819. 69 p.
- Calvert, A.J., 1996. Seismic reflection constraints on imbrication and underplating of the northern Cascadia convergent margin. *Can. J. Earth Sci.* 33, 1294–1307.
- Calvert, A.J., Clowes, R.M., 1991. Seismic evidence for the migration of fluids within the accretionary complex of western Canada. *Can. J. Earth Sci.* 28, 542–556.
- Chaytor, J.D., Goldfinger, C., Dziak, R.P., Fox, C.G., 2004. Active deformation of the Gorda “Plate”: constraining deformation models with new geophysical data. *Geology* 32, 353–356.
- Davis, E.E., Karsten, J.L., 1986. On the cause of the asymmetric distribution of seamounts about the Juan de Fuca Ridge; ridge-crest migration over a heterogeneous asthenosphere. *Earth Planet. Sci. Lett.* 79, 385–396.

- Dziak, R.P., 2006. Explorer deformation zone: evidence of a large shear zone and reorganization of the Pacific–Juan de Fuca–North American triple junction. *Geology* 34, 312–316.
- Flueh, E.R., Fisher, M.A., Bialas, J., Childs, J.R., Klaeschen, D., Kukowski, N., Parsons, T., Scholl, D.W., ten Brink, U., Trehu, A.M., Vidal, N., 1998. New seismic images of the Cascadia subduction zone from cruise SO108–ORWELL. *Tectonophysics* 293, 69–84.
- Fox, C.G., Dziak, R.P., 1999. Internal deformation of the Gorda Plate observed by hydroacoustic monitoring. *J. Geophys. Res.* 104, 17603–17616.
- Fox, C.G., Dziak, R.P., Matsumoto, H., Schreiner, A.E., 1994. Potential for monitoring low-level seismicity on the Juan de Fuca Ridge using fixed hydrophone arrays. *Mar. Tech. Soc. J.* 27, 22–30.
- Furlong, K.P., Schwartz, S.Y., 2004. Influence of the Mendocino triple junction on the tectonics of coastal California. *Annu. Rev. Earth Planet. Sci.* 32, 403–433.
- Gulick, S.P.S., Meltzer, A.S., Clarke Jr., S.H., 1998. Seismic structure of the southern Cascadia subduction zone and accretionary prism north of the Mendocino triple junction. *J. Geophys. Res.* 103, 27207–27222.
- Gulick, S.P.S., Meltzer, A.S., Henstock, T.J., Levander, A., 2001. Internal deformation of the southern Gorda plate: fragmentation of a weak plate near the Mendocino triple junction. *Geology*, 29, 691–694.
- Hacker, B.R., Abers, G.A., Peacock, S.M., 2003a. Subduction factory: 1. Theoretical mineralogy, densities, seismic wave speeds, and H<sub>2</sub>O content. *J. Geophys. Res.* 108, B12029. doi:10.1029/2001JB001127.
- Hacker, B.R., Peacock, S.M., Abers, G.A., Holloway, S.D., 2003b. Subduction factory: 2. Are intermediate-depth earthquakes in subducting slabs linked to metamorphic dehydration reactions? *J. Geophys. Res.* 108, B12030. doi:10.1029/2001JB001129.
- Harris, R.N., Wang, K., 2002. Thermal models of the Middle America Trench at the Nicoya Peninsula, Costa Rica. *Geophys. Res. Lett.* 29, 21–24.
- Hyndman, R.D., Wang, K., 1993. Thermal constraints on the zone of major thrust earthquake failure: the Cascadia subduction zone. *J. Geophys. Res.* 98, 2039–2060.
- Hyndman, R.D., Wang, K., 1995. The rupture of Cascadia great earthquakes from current deformation and thermal regime. *J. Geophys. Res.* 100, 22133–22154.
- Jung, H., Green II, H.W., Dobrzynetskaia, L.F., 2004. Intermediate-depth earthquake faulting by dehydration embrittlement with negative volume change. *Nature* 428, 545–549.
- Kao, H., Wang, K., Chen, R.Y., Wada, I., He, J., Malone, S.D., 2008. Identifying the rupture plane of the 2001 Nisqually, Washington, Earthquake. *Bull. Seis. Soc. Am.* 98, 1546–1558. doi:10.1785/0120070160.
- Kirby, S., Engdahl, R.E., Denlinger, R., 1996. Intermediate-depth intraslab earthquakes and arc volcanism as physical expressions of crustal and uppermost mantle metamorphism in subducting slabs. In: Bebout, G.E., Scholl, D., Kirby, S., Platt, J.P. (Eds.), *Subduction: Top to Bottom. Geophysical Monograph*, vol. 96. American Geophysical Union, Washington DC, pp. 195–214.
- Kodaira, S., Iidaka, T., Kato, A., Park, J.-O., Iwasaki, T., Kaneda, Y., 2004. High pore fluid pressure may cause silent slip in the Nankai Trough. *Science* 304, 1295–1298.
- Louden, K.E., Forsyth, D.W., 1976. Thermal conduction across fracture zones and the gravitational edge effect. *J. Geophys. Res.* 81, 4869–4874.
- Mackay, M.E., Moore, G.F., Cochrane, G.R., Moore, J.C., Kulm, L.D., 1992. Landward vergence and oblique structural trends in the Oregon margin accretionary prism: implications and effect on fluid flow. *Earth Planet. Sci. Lett.* 109, 477–491.
- Malone, S., 2001. Preliminary report on the Mw=6.8 Nisqually, Washington, earthquake of 28 February 2001. *Seism. Res. Lett.* 72, 352–361.
- Masson, D.G., 1991. Fault patterns at outer trench walls. *Mar. Geophys. Res.* 13, 209–225.
- McCrorey, P.A., Blair, J.L., Oppenheimer, D.H., Walter, S.R., 2004. Depth to the Juan De Fuca Slab Beneath the Cascadia Subduction Margin – A 3-D Model for Sorting Earthquakes. U.S. Geological Survey Data Series 91. version 1.0.
- Meade, C., Jeanloz, R., 1991. Deep-focus earthquakes and recycling of the water into the earth's mantle. *Science* 252, 68–72.
- Moore, J.C., Vrolijk, P., 1992. Fluids in accretionary prisms. *Rev. Geophys.* 30, 113–135.
- Nedimović, M.R., Hyndman, R.D., Ramachandran, K., Spence, G.D., 2003a. Reflection signature of seismic and aseismic slip on the northern Cascadia subduction interface. *Nature* 424, 416–420.
- Nedimović, M.R., Mazzotti, S., Hyndman, R.D., 2003b. Three-dimensional structure from feathered two-dimensional seismic reflection data; the eastern Nankai trough. *J. Geophys. Res.* 108 (B10), 1–14. doi:10.1029/2002JB001959 2456.
- Nedimović, M.R., Carbotte, S.M., Harding, A.J., Detrick, R.S., Canales, J.P., Diebold, J.B., Kent, G.M., Tischer, M., Babcock, J.M., 2005. Frozen magma lenses below the oceanic crust. *Nature* 436, 1149–1152.
- Nedimović, M.R., Carbotte, S.M., Diebold, J.B., Harding, A.J., Canales, J.P., Kent, G.M., 2008. Upper crustal evolution across the Juan de Fuca ridge flanks. *Geochem. Geophys. Geosyst.* 9, 1–23. doi:10.1029/2008GC002085 Q09006.
- Peacock, S.M., 1990. Fluid processes in subduction zones. *Science* 248, 329–337.
- Peacock, S.M., 2001. Are the lower planes of double seismic zones caused by serpentine dehydration in subducting oceanic mantle? *Geology* 29, 299–302.
- Raleigh, C.B., Paterson, M.S., 1965. Experimental deformation of serpentinite and its tectonic implications. *J. Geophys. Res.* 70, 3965–3985.
- Ranero, C.R., Phipps Morgan, J., McIntosh, K., Reichert, C.B., 2003. Bending-related dilatancy and the mantle serpentinization at the Middle America trench. *Nature* 425, 367–373.
- Rogers, G.C., Crosson, R.S., 2002. Intraslab earthquakes beneath Georgia Strait/Puget Sound. In: Kirby, S., Wang, K., Dunlop, S. (Eds.), *The Cascadia Subduction Zone and Related Subduction Systems. U.S. Geological Survey Open-File Report 02-328 and Geological Survey of Canada Open-File 4350*, pp. 65–68.
- Seno, T., Yoshida, M., 2004. Where and why do large shallow intraslab earthquakes occur? *Phys. Earth Planet. Inter.* 141, 183–206.
- Shibley, T.H., Moore, G.F., Bangs, N.L., Moore, J.C., Stoffa, P.L., 1994. Seismically inferred dilatancy distribution, northern Barbados Ridge decollement: implications for fluid migration and fault strength. *Geology* 22, 411–414.
- Tatsumi, Y., Eggins, S., 1995. *Subduction Zone Magmatism*. Blackwell Science, Oxford.
- Ulmer, P., Trommsdorff, V., 1995. Serpentine stability to mantle depths and subduction-related magmatism. *Science* 268, 858–861.
- Underwood, M.B., Hoke, K.D., Fisher, A.T., Davis, E.E., Giambalvo, E., Zühlsdorff, L., Spinelli, G.A., 2005. Provenance, stratigraphic architecture, and hydrogeologic influence of turbidites on the mid-ocean ridge flank of northwestern Cascadia Basin, Pacific Ocean. *J. Sediment. Res.* 75, 149–164.
- Vallée, M., Bouchon, M., Schwartz, S.Y., 2003. The 13 January 2001 El Salvador earthquake: a multidata analysis. *J. Geophys. Res.* 108, 2203. doi:10.1029/2002JB001922.
- Wada, I., Wang, K., He, J., Hyndman, R.D., 2008. Weakening of the subduction interface and its effects on surface heat flow, slab dehydration, and mantle wedge serpentinization. *J. Geophys. Res.* 113, B04402. doi:10.1029/2007JB005190.
- Wang, K., Mulder, T., Rogers, G.C., Hyndman, R.D., 1995. Case for very low coupling stress on the Cascadia subduction fault. *J. Geophys. Res.* 100, 12907–12918.
- Wang, K., He, J., Davis, E.E., 1997. Transform push, oblique subduction resistance, and intraplate stress of the Juan de Fuca plate. *J. Geophys. Res.* 102, 661–674.
- Wells, R.E., Blakely, R.J., Weaver, C.S., 2002. Cascadia microplate models and within-slab earthquake. In: Kirby, S., Wang, K., Dunlop, S. (Eds.), *The Cascadia Subduction Zone and Related Subduction Systems. U.S. Geological Survey Open-File Report 02-328 and Geological Survey of Canada Open-File 4350*, pp. 17–23.
- Wilson, D.S., 1988. Tectonic history of the Juan de Fuca ridge over the last 40 million years. *J. Geophys. Res.* 93, 11863–11876.
- Wilson, D.S., 1993. Confidence intervals for motion and deformation of the Juan de Fuca plate. *J. Geophys. Res.* 98, 16053–16071.
- Wilson, D.S., 2002. The Juan de Fuca plate and slab—isochron structure and Cenozoic plate motions. In: Kirby, S., Wang, K., Dunlop, S. (Eds.), *The Cascadia Subduction Zone and Related Subduction Systems. U.S. Geol. Survey Open-File Report 02-328 and Geological Survey of Canada Open-File 4350*, pp. 9–12.
- Wong, I.G., 2004. Low potential for large intraslab earthquakes in the central Cascadia subduction zone. *Bull. Seis. Soc. Am.*, 95, 1880–1902.
- Yamasaki, T., Seno, T., 2003. Double seismic zone and dehydration embrittlement of the subducting slab. *J. Geophys. Res.* 108, B42212. doi:10.1029/2002JB001918.